# Supporting Information

# K-birnessite-$MnO_2$/hollow mulberry-like carbon complexes with stabilized and superior rate performance for aqueous magnesium ion storage

Xueli Chen[a,b], Lu Han [b,*], Yanjiang Li[b], Guangzhen Zhao[b], Guoliang Gao[b], Lianghao Yu[b], Xiuyang Shan[b], Xusheng Xie[b], Xinjuan Liu[c], Guang Zhu [a,b,*]

[a] School of Materials Science and Engineering, Anhui Polytechnic University, Wuhu 241000, PR China

[b] Key Laboratory of Spin Electron and Nanomaterials of Anhui Higher Education Institutes, Suzhou University, Suzhou 234000, PR China

[c] School of Materials and Chemistry, University of Shanghai for Science and Technology, Shanghai 200093, P.R. China

* *Corresponding author: Lu Han (982563331@qq.com);*

*Guang Zhu (guangzhu@ahszu.edu.cn)*

## Chemicals and Regents

The polyacrylonitrile (PAN, Mw = 150000) was purchased from Sigma-Aldrich (Shanghai) Trade Co. Ltd. The $SiO_2$ nanospheres were bought from Ruijiang Nanomaterial Technology Co. Concentrated hydrochloric acid (HCl) was purchased from Shanghai Zhenqi Chemical Reagent Co., Ltd. (Shanghai, China). The lithium fluoride (LiF) was purchased from Aladdin Shanghai Co., Ltd. (Shanghai, China). The N, N-dimethylformamide (DMF, AR), $KMnO_4$, carbon black, polyvinylidene fluoride (PVDF), and 1-methyl-2-pyrrolidone (NMP) were all purchased from Sinopharm Chemical Reagent Co., Ltd. All reagents were directly used as received without further purification.

## Materials Characterization

Field emission scanning electron microscopy (SEM, Hitachi, S-4800) with energy dispersive spectrometer (EDS, Bruker Quantax-400) and transmission electron microscope (TEM, JEM-2100F, JEOL) were used to examine the morphology, structure, and element distribution of the materials. Measurements of the sample's microstructure was made using an X-ray diffractometer (XRD, Rigaku Smart Lab, TM 9kW, Cu-K, = 1.5418A, 30 kV, 25 mA, scanning range 5-90°), a Raman spectrometer (Raman, Horibo-H800, tested under 532 nm excitation light). Measurements of the sample's specific surface area and pore distribution were made using a physical adsorption instrument. In order to suit the XPS test results, XPS Peak 4.1 software was

used to assess the material element composition and valence states using X-ray photoelectron spectroscopy (XPS, Esca lab 250Xi).

**Electrochemical Measurements.**

An apparatus with three electrodes was used to gauge electrochemical characteristics of the samples. A composite K-$MnO_2$/HMC material coated on graphite paper served as the working electrode, a saturated calomel electrode served as the reference electrode, and a Pt rod served as the opposing electrode. A little more than 1 mg of K-$MnO_2$/HMC composites are present in the working electrode, which has a geometric surface area of 1 $cm^2$. As the electrolyte solution, we utilized 1.0 M magnesium sulfate solution. An electrochemical workstation was used to measure cyclic voltammetry (CV), galvanostatic charge-discharge curves (GCD), and electrochemical impedance spectroscopy (EIS) (AUTOLAB PGSTA302N). The voltage range for CV is -0.5 to 1.3 V (versus Hg/HgO), and the scan rates range from 2 to 50 mV $s^{-1}$. The voltage range for GCD is -0.5 to 1.3 V (versus Hg/HgO), and the current density ranges from 0.2 to 10 A $g^{-1}$. The frequency range used for the electrochemical impedance spectroscopy was 1 MHz to 0.1 Hz. The K-$MnO_2$/HMC electrode was made by combining N-methyl-2-pyrrolidone with 80 weight percent K-$MnO_2$/HMC composite material, 10 weight percent acetylene black, and 10 weight percent polyvinylidene fluoride (PVDF) (NMP). Two graphite electrodes with carbon coatings were combined to form an asymmetric supercapacitor. The identical procedure was used to make the AC electrode, but instead of mixing HMC and $MnO_2$, the AC electrode was made by mixing AC. The electrolyte is a 1 M aqueous solution of

magnesium sulfate. An electrochemical workstation was used to measure the two-electrode system's CV and GCD (AUTOLAB PGSTA302N). The active substance mass was used to compute all working current densities.

**Related calculations.** For the three-electrode and two-electrode systems, the specific capacitance ($C_F$, F $g^{-1}$; C, mA h $g^{-1}$) was calculated from the GCD curves according to the following equation:

$$C_F = \frac{I \times \Delta t}{m \times \Delta V}$$

$$C_F = \frac{I \times \Delta t}{m \times 3.6}$$

where I, ΔV, m and t refer to the current (A), potential window (V), mass of active material (g) and discharge time (s), respectively.

For the two-electrode system, the energy density (E, Wh $Kg^{-1}$) and power density (P, W $Kg^{-1}$) were calculated according to the following equations:

$$E = \frac{C_F \times \Delta V^2}{2 \times 3.6}$$

$$P = \frac{3600 \times E}{\Delta t}$$

where $C_F$, ΔV, and Δt refer to the specific capacitance (F $g^{-1}$), potential window (V), and discharge time (s), respectively.

Formula S1

$$4KMnO_4 + 3C + 2H_2SO_4 \longleftrightarrow 4MnO_2 + 3CO_2 + 2K_2SO_4 + 2H_2O$$

Formula S2

$i(V) = k_1v$ (capacitive controlled) + $k_2v^{1/2}$ (diffusive controlled)

Table S1 Specific surface areas and pore parameters of as-prepared HMC, K-$MnO_2$, K-$MnO_2$/HMC electrodes.

| Sample | Specific surface area ($m^2$ $g^{-1}$) | Volume ($cm^3$ $g^{-1}$) | Average pore size (nm) |
|---|---|---|---|
| HMC | 43.3 | 0.055 | 5.073 |
| K-$MnO_2$ | 56.1 | 0.095 | 6.811 |
| K-$MnO_2$/HMC | 57.8 | 0.057 | 3.967 |

Table S2 Comparison of the performances between K-$MnO_2$/HMC and other electrode materials for aqueous Mg-ion system reported in the literature.

| Materials | Electrolyte | Voltage | Energy density (Wh $kg^{-1}$) | Energy density (kW $kg^{-1}$) | Cycling stability | Ref |
|---|---|---|---|---|---|---|
| K-$MnO_2$ | 1 M $MgSO_4$ | 0-1.8 V | 85.2 | 360 | 96.7% after 20000 cycles at 5 A $g^{-1}$ | 1 |
| Mg-OMS-2/Graphene | 0.5 M Mg $(NO_3)_2$ | 0-2.0 V | 46.9 | / | 93% after 300 cycles at 0.1 A $g^{-1}$ | 2 |
| Mg-OMS-1/Graphene | Mg $(NO_3)_2$ | 0-0.8 V | / | / | 98.6% after 800 cycles at 0.1 A $g^{-1}$ | 3 |
| Co- $MnO_2$ | 1 M $MgSO_4$ | 0-1.8 V | 79.6 | 360 | 98.4% after 15000 cycles at 5 A $g^{-1}$ | 4 |
| MXene/rGO | 1M $Na_2SO_4$ and 1M $MgSO_4$ | -0.5-0.5 V | / | / | 87% after 10000 cycles at 10 A $g^{-1}$ | 5 |
| δ-$MnO_2$ | $MgSO_4$ and Mg $(NO_3)_2$ | 0-1.8 V | 103.9 | 3680 | 58.3% after 1000 cycles at 6 A $g^{-1}$ at -20 ℃ | 6 |
| HAQ-COF | 1 M $MgSO_4$ | 0-1.5 V | / | / | 75% after 6000 cycles at 5 A $g^{-1}$ | 7 |
| **K-$MnO_2$/HMC** | **1 M $MgSO_4$** | **0-2.6 V** | **111.1** | **505** | **97.3% after 5000 cycles at 10 A $g^{-1}$** | **This work** |

Table S3 Mn and O species content (at%) of K-$MnO_2$ and K-$MnO_2$/HMC based on XPS results.

| Sample | $Mn^{3+}$ | $Mn^{4+}$ | Mn-O | Mn-O-C |
|---|---|---|---|---|
| K-$MnO_2$ | 68.0% | 32.0% | 65.1% | - |
| K-$MnO_2$/HMC | 53.4% | 46.6% | 47.2% | 32.6% |

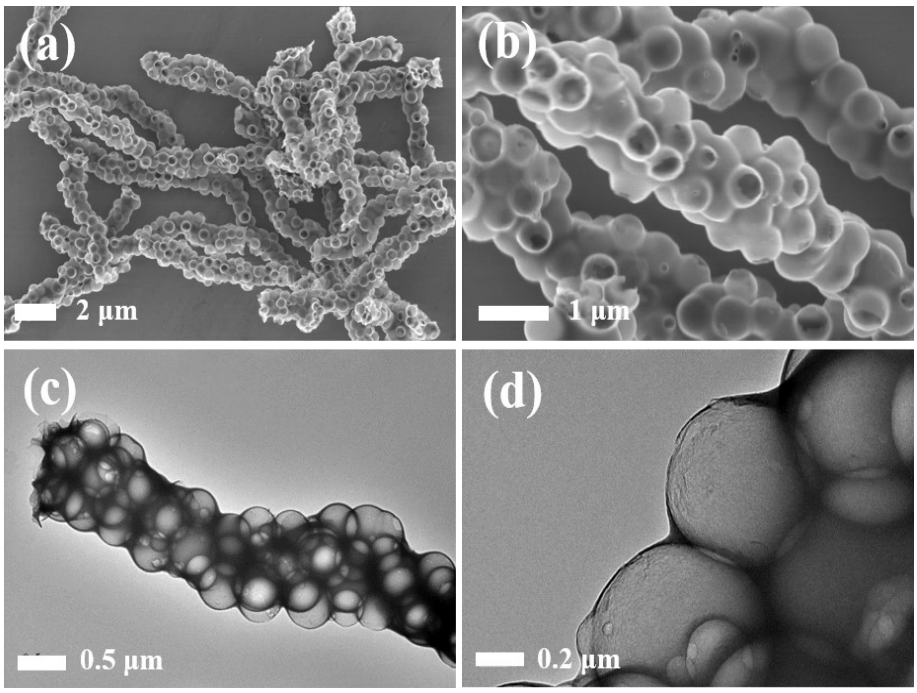


Fig. S1 SEM (a, b) and TEM (c, d) images of HMC.

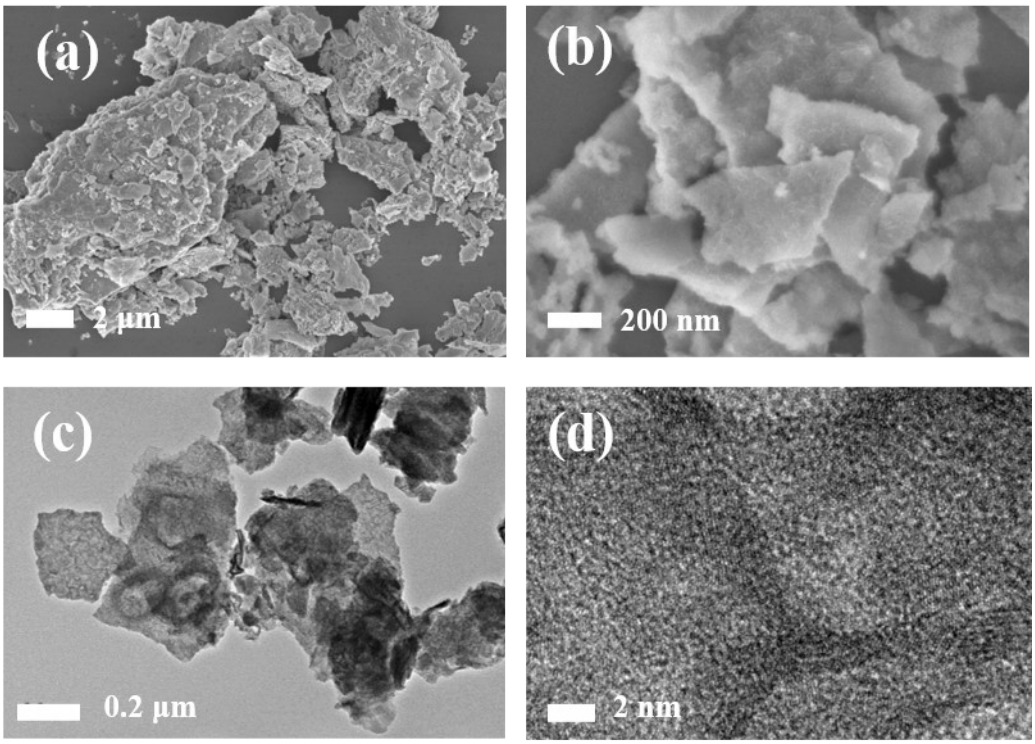


Figure. S2 SEM (a, b) and TEM (c, d) images of K-$MnO_2$.

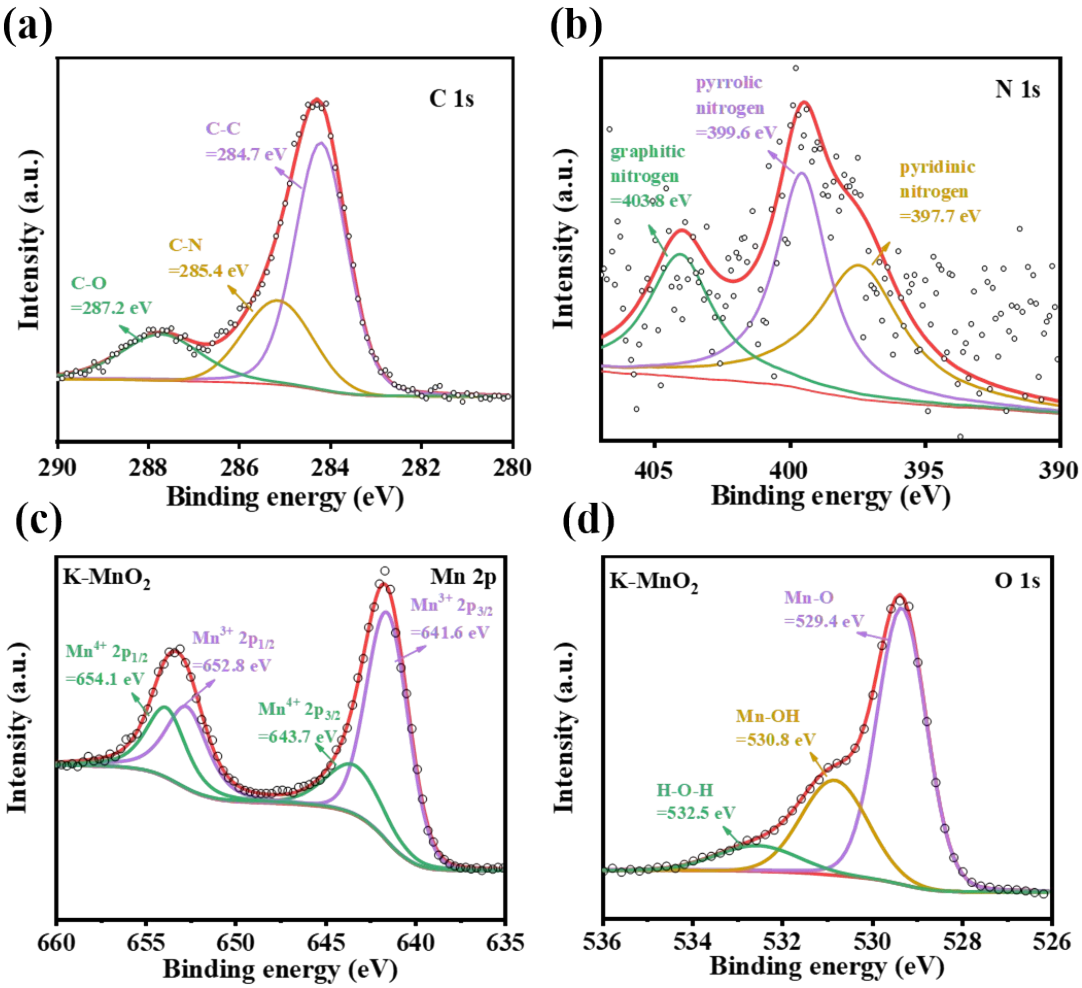


Figure. S3 (a) C 1s, (b) N 1s XPS spectra of K-$MnO_2$/HMC. (c) Mn 2p, (d) O 1s XPS spectra of K-$MnO_2$.

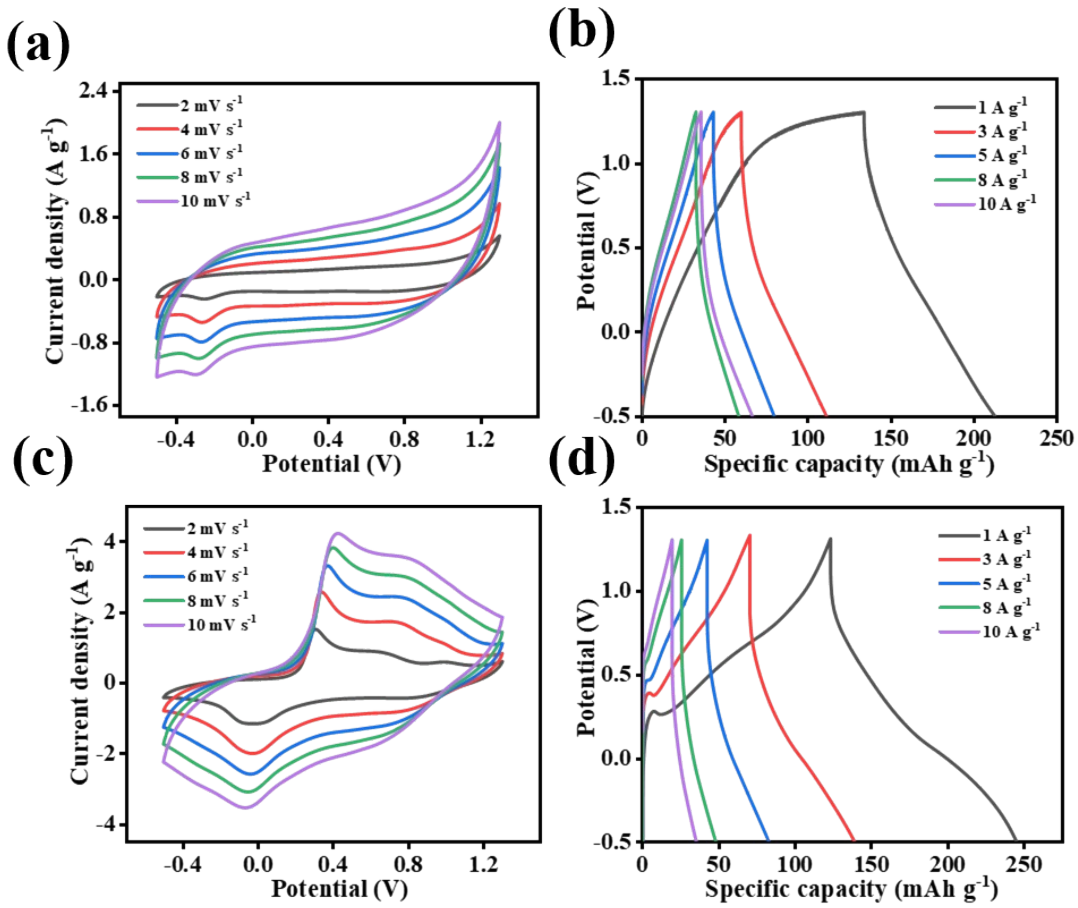


Figure. S4 (a, b) CV and GCD curves of HMC. (c, d) CV and GCD curves of K-$MnO_2$ at various scan rates current densities.

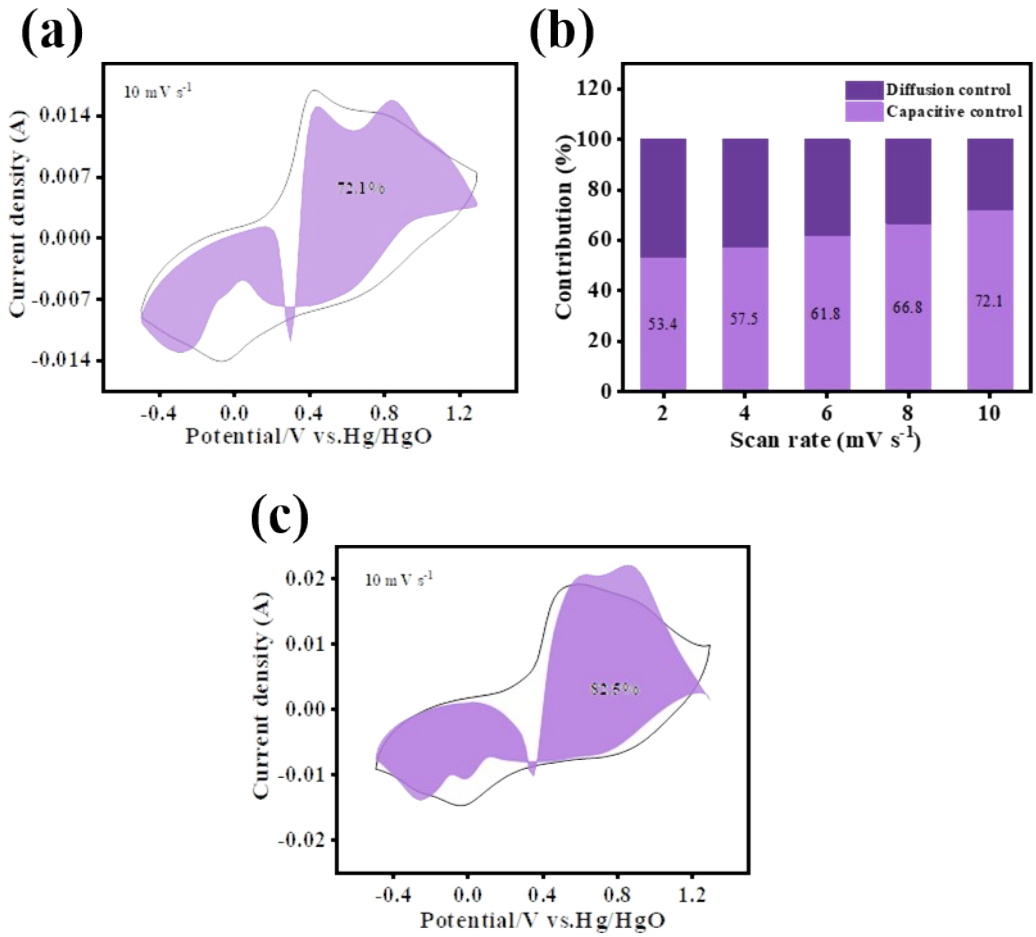


Figure. S5 (a) CV curve with the capacitive contribution at a scan rate of 10 mV $s^{-1}$, (b) Percentage of capacity contribution at various scan rates for K-$MnO_2$ electrode. (c) CV curve with the capacitive contribution at a scan rate of 10 mV $s^{-1}$ for K-$MnO_2$/HMC.

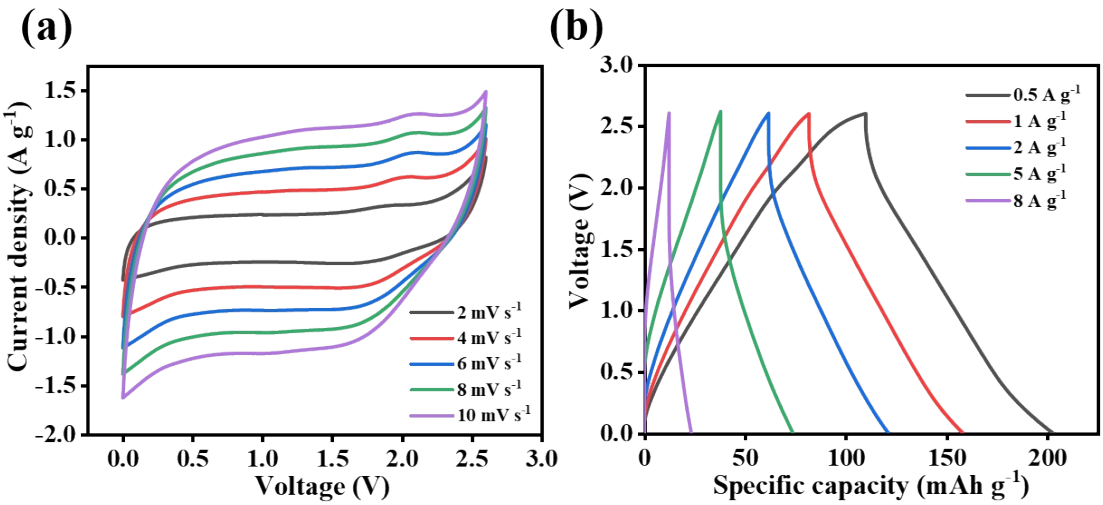


Figure. S6 (a, b) CV and GCD curves of K-$MnO_2$ electrode at different scan rates and current densities in a voltage window of 2.6 V.

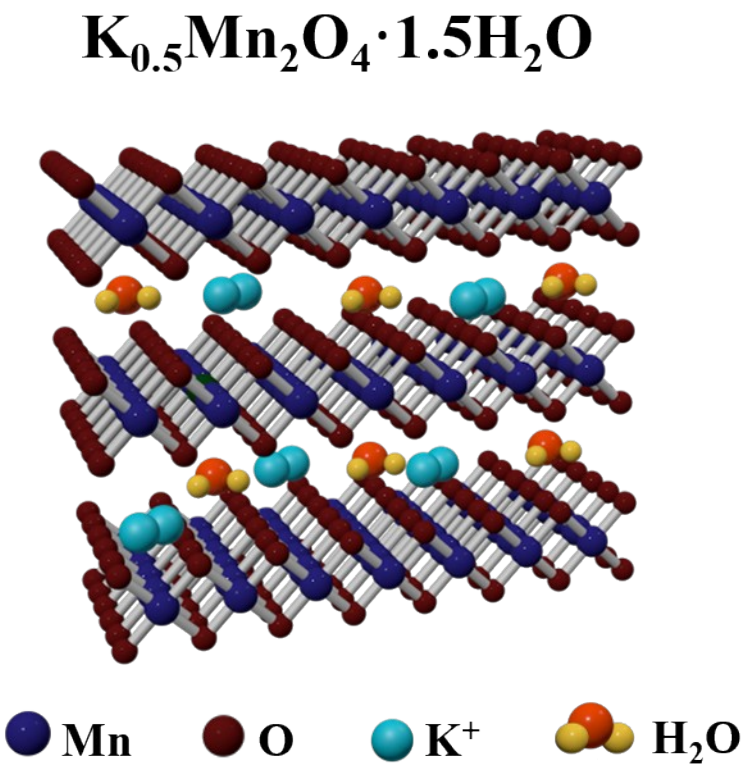


Figure. S7 Chemical formula and structural formula of K-$MnO_2$.

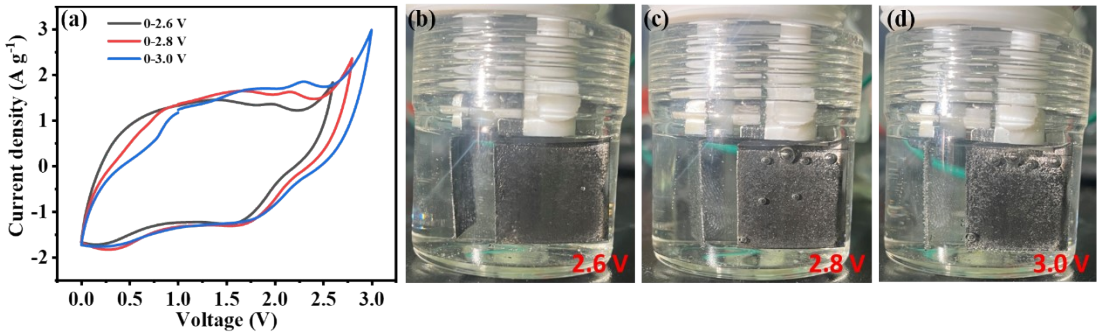


Figure. S8 The (a) CV and (b-d) electrode surface bubbling for K-$MnO_2$/HMC at different voltage windows.

## References


1. L. Xu, G. Pan, J. Wang, J. Li, Z. Gong, T. Lu and L. Pan, Sustainable Energy & Fuels, 2022, 6, 5290-5299.
2. H. Zhang, K. Ye, K. Zhu, R. Cang, X. Wang, G. Wang and D. Cao, ACS Sustainable Chemistry & Engineering, 2017, 5, 6727-6735.
3. H. Zhang, D. Cao, X. Bai, H. Xie, X. Liu, X. Jiang, H. Lin and H. He, ACS Sustainable Chemistry & Engineering, 2019, 7, 6113-6121.
4. L. Xu, G. Pan, C. Yu, J. Li, Z. Gong, T. Lu and L. Pan, Inorganic Chemistry Frontiers, 2023, 10, 1748-1757.
5. M. Gyu Jung, G. Sambhaji Gund, Y. Gogotsi and H. Seok Park, Batteries & Supercaps, 2020, 3, 354-360.
6. G. Yang, G. Qu, C. Fang, J. Deng, X. Xu, Y. Xie, T. Sun, Y. Zhu, J. Zheng and H. Zhou, Green Energy & Environment, 2022, DOI: 10.1016/j.gee.2022.09.004.
7. G. Zou, Z. Tian, V. S. Kale, W. Wang, S. Kandembeth, Z. Cao, J. Guo, J. Czaban-Jóźwiak, L. Cavallo, O. Shekhah, M. Eddaoudi and H. N. Alshareef, Advanced Energy Materials, 2022, 13 2203193.